buildings

MDPI

Article

Enhancing Daylight and Energy Efficiency in Hot Climate Regions with a Perforated Shading System Using a Hybrid Approach Considering Different Case Studies

Basma Gaber [1], Changhong Zhan [1], Xueying Han [1,*], Mohamed Omar [2,3] and Guanghao Li [4]

[1] Key Laboratory of Cold Region Urban and Rural Human Settlement Environment Science and Technology, School of Architecture and Design, Harbin Institute of Technology, Ministry of Industry and Information Technology, Harbin 150001, China; basmagaber@stu.hit.edu.cn (B.G.); zhan.changhong@hit.edu.cn (C.Z.)
[2] State Key Laboratory of Robotics and System, Harbin Institute of Technology, Harbin 150001, China; mohamed_omar@mans.edu.eg
[3] Production and Mechanical Design Engineering Department, Faculty of Engineering, Mansoura University, Mansoura 35516, Egypt
[4] School of Architecture and Planning, Shenyang Jianzhu University, Shenyang 110168, China; guanghao.li@sjzu.edu.cn
* Correspondence: hanxueying119@hit.edu.cn

Abstract: Direct sunlight causes glare and reduces indoor daylight quality, making shading systems essential. This study proposes and validates a perforated shading screen (PSS) to enhance daylighting and energy efficiency. A hybrid approach integrating parametric modeling, machine learning, multi-criteria decision-making (MCDM), and genetic algorithm (GA) is used to optimize the design incorporating architects' preferences. The Analytic Network Process (ANP) is used to assign weights to performance metrics while accounting for interdependencies. The study evaluates PSS performance in three hot climate regions—Cairo, Riyadh, and Kuching—on both south and west elevations, comparing it to traditional fins. Results show that PSS consistently outperforms fins, significantly improving daylight and energy performance. The Useful Daylight Illuminance (UDI) increased by up to 105.32%, Continuous Daylight Autonomy (CDA) by up to 11.87%, while Annual Solar Exposure (ASE), Solar Gain (SG), and Energy Use Intensity (EUI) were reduced by up to 100%, 88.07%, and 45.2%, respectively. To validate the findings, the optimal PSS design from a selected case study was 3D-printed and experimentally tested. Results confirmed enhanced daylight distribution and reduced glare, improving occupant comfort. The proposed PSS offers an effective shading solution adaptable to various climates, balancing daylighting needs and energy efficiency.

Keywords: perforated shading screens; multi-objective optimization; MCDM; shading systems; hot climates; daylight performance

Academic Editor: Vincenzo Costanzo

Received: 2 March 2025
Revised: 16 March 2025
Accepted: 18 March 2025
Published: 20 March 2025

Citation: Gaber, B.; Zhan, C.; Han, X.; Omar, M.; Li, G. Enhancing Daylight and Energy Efficiency in Hot Climate Regions with a Perforated Shading System Using a Hybrid Approach Considering Different Case Studies. *Buildings* **2025**, *15*, 988. https://doi.org/10.3390/buildings15060988

1. Introduction

There has been a trend in recent years towards the construction of high-rise glazed towers [1] as the preferred architectural style. However, these buildings can become heat traps due to high annual solar radiation, leading to significant visual and thermal discomfort [2]. Hence, they are frequently unsuitable for hot regions [3]. To optimize visual comfort and minimize glare from excessive lighting, it is important to utilize shading devices [4,5]. Shading systems help regulate solar radiation and maintain the building's energy balance, especially in hot climates. Thus, choosing the right shading system early in

the design process is crucial [6,7]. Fixed shading systems are an essential component of architectural design and continue to attract considerable attention from researchers. This interest is driven by their simplicity, low cost, ease of installation, minimal maintenance, and passive operation. Small refinements in the shading system's design during the early planning stages can greatly improve the efficiency of the building's energy, particularly in hot climates [8,9]. These systems offer a cost-effective alternative to dynamic shading systems, which often require higher investments and ongoing maintenance [10].

Perforated shading screens (PSS) are gaining popularity among architects, especially those focused on sustainable building envelopes [11]. Beyond their visual appeal, these screens play a crucial role in enhancing environmental performance by effectively filtering and distributing natural light within a space [12]. PSS are particularly well-suited for fully glazed façades, acting as a second skin with opaque perforations that block direct sunlight while preserving outdoor views [13]. As architecture evolves from traditional to modern styles, these shading systems have become a preferred choice, offering both aesthetic and functional advantages for controlling sunlight and improving indoor environments [14].

Designing efficient shading systems for hot climates is a complex process that requires balancing multiple factors while managing conflicting design constraints. As sustainability, cost efficiency, and strict project deadlines become increasingly important, façade design grows more intricate [15]. Additionally, developing complex geometric patterns that optimize both performance and affordability poses a significant challenge, often leading to design inaccuracies [16]. The intricate structure of perforated shading screens (PSS) further complicates analysis. Even a slight modification in a single pattern parameter can alter the shape, impacting both energy efficiency and visual performance. The large number of design variables creates an extensive range of possible configurations, making it impractical to evaluate every variation. As a result, simulation processes become time-intensive and costly, often requiring months to complete [17].

Several studies have explored various PSS designs and design approaches to enhance building performance. Table 1 provides a summary of the recent studies, organized chronologically according to their publication dates.

Parametric design is used extensively in geometrical patterns for aesthetics and environmental control, particularly in regard to the management of natural light, temperature, and visual comfort [18]. The Rhinoceros® version 7 with Grasshopper software v7 and its related plug-ins are currently used by most researchers as a tool for parametric models [19]. Some studies examined the impact of PSS and focused on the historical aspect (Traditional Mashrabiya) on a single objective, such as visual comfort [20,21]. Emami et al. [20] analyzed fixed Persian geometric patterns as shading systems, focusing on daylight autonomy. Other studies have focused on thermal performance. For example, Taki et al. [22] examined traditional Mashrabiya-inspired PSS, highlighting its energy efficiency and cultural significance in Saudi Arabia. However, their study overlooked key visual comfort factors, such as daylight distribution and glare control. Bande et al. [23] investigated Mashrabiya-PSS in housing projects in the UAE by studying Energy consumption, reporting up to 60% electricity savings in the early design phase. As mentioned earlier, the design process of PSS involves balancing multiple objectives. To achieve optimal designs, parametric simulations must be integrated with multi-objective optimization algorithms.

Table 1. Summary of the recent previous studies.

No.	Study	Location	Performance			Method	Shading	Orientation	Validation	MCDM
			Daylight	Glare	Energy and Thermal Comfort					
1	[24]	Saudi Arabia (BWh) *	DA	DGP	kWh/m^2	Simulation	Contemporary Mashrabiya	S, E, W, N	x	x
2	[20]	Michigan (Dfa)	DA	--	--	Simulation and Measurements	Contemporary Mashrabiya	S	√	x
3	[14]	Seville, Spain (Csa)	Daylit area	--	Annual energy	Simulation and The Design of Experiments using Orthogonal Arrays	Simple Geometry (circle, triangle, hexagon)	S	x	x
4	[25]	Iran, Tehran (BSk)	sDA	ASE	--	Optimization-GA	Kinetic Rosetta Pattern	S	x	x
5	[21]	Egypt (BWh)	Point time illuminance	--	--	Simulation and measurement	Fixed IGPs	--	√	×
6	[26]	Catalonia, Spain (Csa)	SDA	ASE	--	MOO NSGA II	Modern Design	S	x	x
7	[27]	Taipei (Cfa)	DA	ASE	--	Prediction with metamodel using ANN	Simple Geometry (circle)	S	x	x
8	[28]	UAE (BWh)	UDI	--	Solar radiation	Simulation	Fixed Rosetta	--	x	x
9	[29]	semi-arid climate (BSh)	UDI, sDA	--	EUI	Grid-based simulation and general morphological analysis	Hexagonal shape of IGP with Orosi windows	S	x	x
10	[23]	UAE (BWh)	--	--	KWH solar radiation	simulation	Six triangular units	S	x	x
11	[22]	Saudi Arabia (BWh)	DF		KW/h, solar gain	simulation	Fixed Traditional Mashrabiya	S	x	x
12	[30]	Turkey (Csa)	sDA, UDI	ASE, DGP	--	Simulation	semi-regular and demi-regular tessellations	S	x	x
13	[31]	Istanbul (Csa)	sDA, UDI	DGP	--	Simulation	Dynamic origami	S	x	x

Table 1. *Cont.*

No.	Study	Location	Performance			Method	Shading	Orientation	Validation	MCDM
			Daylight	Glare	Energy and Thermal Comfort					
14	[32]	Isfahan (BWk)	UDI, sDA	sGA	EUI	Simulation	PSS, louvers, eggcrate	S, SW, W, NW, N, NE, E, SE	x	Multi-Attribute Utility Theory (MAUT)
15	[13]	Wuhan, China (Cfa)	UDI, sDA, Temporal uniformity factor (TUF)	SDG	--	Simulation study-Data Envelopment Analysis	Non-uniform PPS	S	x	x

* Climate: Tropical Monsoon (Am), Tropical rainforest (Af), Continental Subarctic (Dfc), Humid continental: (Dfb), Hot Summer Continental (Dfa), Temperate (Cfb), Humid Subtropical Climate (Cfa), Warm desert (BWh), Marine West Coast (Cfb), Mild, Semi-humid (Csa), Tropical, savanna (Aw), Semi-arid (BSh).

Some studies started to consider multi objectives in the design process. In refs. [25,26], they utilized Rosetta patterns with internal louvers to optimize ASE and SDA using genetic algorithms in Grasshopper to achieve LEED v4 certification. Huang et al. [13] examined non-uniform perforation dynamic patterns in solar screens and their impact on daylight performance metrics (UDI, sDA, ASE, TUF, sDG). However, the studies excluded building energy use from their analysis. Hosseini et al. [29] used general morphological analysis (GMA) and a kinetic design with strategy to optimize multilayer of hexagonal Pattern with colorful glass compositions, identifying the best color combinations for enhancing UDI, EUDI, sDA. While considering multiple objectives significantly improves PSS design performance, the process is time-consuming. Typically, optimization is carried out in a step-by-step manner, which limits the ability to explore a broad range of design variables.

Some studies started to investigate the employment of machine learning methods, as in ref. [27]. They applied artificial neural networks (ANNs), to reduce simulation time while analyzing PSS with circular hole-shaped façades considering daylight autonomy (DA) and annual solar exposure (ASE). Wen et al. [33] investigated four shading techniques using the ANN and multi-objective genetic algorithm. However, their study relied on datasets collected through field surveys, a process that is both time-intensive and challenging, particularly when striving for optimal performance [34]. Employing machine learning regression models as fitness functions helps in speeding up the optimization process and allows for searching for a wide range of design variables. Although significant improvements have been made to the PSS design process, selecting the optimal design remains a complex task. This is due to the need to consider multiple, often conflicting objectives. Balancing factors such as energy efficiency, daylight distribution, aesthetic appeal, and cost-effectiveness require careful analysis and decision-making. As a result, identifying the best design is not straightforward and involves navigating a delicate trade-off between competing goals.

Multi-criteria decision-making (MCDM) serves as an effective approach for optimizing shading system design by systematically evaluating and ranking various options. It enables the prioritization of key objectives and facilitates the identification of the most suitable design solution [35]. Kangazian et al. [32] analyzed various shading designs, such as PSS, louvers, and eggcrate, with different orientations in cold desert climates. They employed the Multi-Attribute Utility Theory (MAUT) approach to evaluate these designs, ultimately identifying the most optimal options for each orientation. However, the study notes for selecting the best design from a predefined set may not always be sufficient. In some instances, it is crucial to broaden the parameter scope and optimize it to determine the most effective design. Additionally, the accuracy of the MAUT method depends heavily on the selected attribute utility functions, which can significantly impact the results. Based on the findings from this literature review on PSS shading systems, the following gaps have been identified:

- Most studies focus primarily on south-facing (S) orientations, with fewer investigations into other cardinal directions [32,36], and most studies do not account for how shading performance varies across different latitudes, climates, or regional solar exposure patterns. This limits the global applicability of the findings.
- Only a few studies include fabrication and validation [20,21,36], meaning most research relies solely on simulations or theoretical models without physical prototyping or real-world testing. This lack of experimental validation raises questions about the practical applicability and accuracy of the proposed shading systems.
- In the design and optimization of PSS, the chosen patterns varied based on the context of each study, encompassing modules of Islamic Geometric Patterns (IGPs) such as Rosetta, as well as simple geometric shapes like circles, squares, and hexagons, along

with folded geometry [29]. In contrast, other patterns, such as the star pattern, received comparatively less focus.

- Additionally, the current literature predominantly emphasizes daylight performance, while thermal performance is less explored [13,25]. Most studies focused on the improvement of lighting through UDI [30,37], neglecting other metrics that could indicate the presence of glare. In particular, ASE (Annual Sunlight Exposure) was often overlooked, despite its importance in assessing excessive sunlight that may cause visual discomfort and reduce indoor lighting quality.
- Furthermore, existing studies often overlook architects' preferences and fail to account for the interdependencies between performance metrics. Traditional MCDM methods, such as Analytic Hierarchy Process (AHP), assume independence among criteria. In contrast, ANP can account for interdependence and feedback between criteria and alternatives, making it particularly suitable for complex decision-making scenarios. By incorporating ANP, designers and researchers can better capture the dynamic relationships between various design parameters, leading to more robust and informed decisions in shading system selection. This approach can ultimately enhance the performance, sustainability, and adaptability of building façades in diverse climatic conditions.

This research aims to develop a new perforated shading screen (PSS) design using star patterns, inspired by the traditional Middle Eastern Mashrabiya style, which reflects the cultural heritage of different hot climate regions. The new design will be easy to fabricate and validate, offering both aesthetic appeal and enhanced performance. The study will assess its effectiveness across various hot climate regions, considering both south and west-facing elevations to test its applicability and general performance. The optimization and design selection process considers five key performance measures: Useful Daylight Illuminance (UDI), Energy intensity use (EUI), Annual sun exposure (ASE), Continuous Daylight Autonomy (CDA), and Solar gains (SG). These metrics help evaluate the effectiveness of the shading system in terms of daylight distribution, energy efficiency, solar exposure control, and thermal performance. Additionally, the design will be compared with the commonly used vertical fins shading system in hot climate regions. To ensure an effective design process, a robust framework will be employed, integrating parametric modeling, machine learning, multi-criteria decision-making (MCDM), and genetic algorithms (GA) for optimization. The Analytic Network Process (ANP) will be used to assign weights to performance metrics, incorporating architects' preferences and considering interdependencies between them. To demonstrate the feasibility of the proposed design, it will be 3D printed and experimentally tested under 15 standard sky conditions to evaluate its impact on occupants.

2. Materials and Methods

2.1. The Proposed PSS Design

The proposed shading system is a Mashrabiya-inspired PSS. Mashrabiya is a frame of wood that is employed to cover a window aperture and augment the visual attractiveness of the building, and it also acts as a natural humidifier [38] (see Figure 1a). Mashrabiya has many shapes starting from simple hexagons to more complex polygons and stars, which are further classified into 8-, 10-, and 12-point (see Figure 1b). Mashrabiya is one of the most iconic cultural and historical elements in many hot climate regions like the selected case studies [39], which are Cairo (Egypt), Riyadh (Saudi Arabia), and Kuching (Malaysia), making the Mashrabiya PSS a highly suitable choice. Art and architecture are essential in preserving cultural heritage and shaping individual identity.

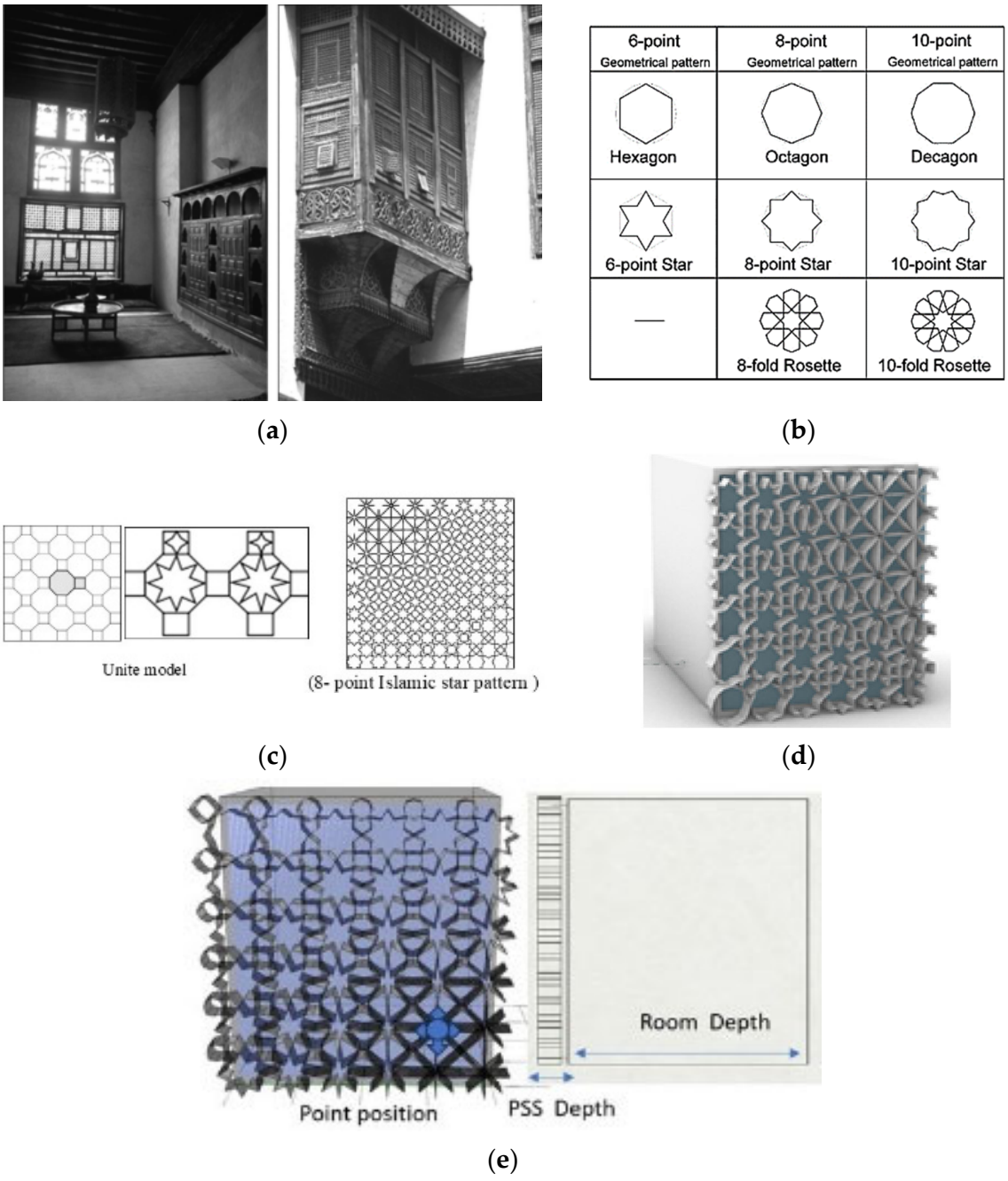

Figure 1. The proposed PSS shading. (**a**) The historical Mashrabiya. (**b**) Most common geometric patterns. (**c**) The used star pattern. (**d**) The shading 3D model. (**e**) PSS Design variables.

The shading system Is shown In Figure 1c,d. The proposed Mashrabiya-inspired PSS consists of an 8-point star, and its parameters are shown in Figure 1e. The technique of pattern generation forms using Hankin's method [40]. Most perforated shading screens are typically manufactured using laser cutting, CNC machining, or water jet cutting [41], all of which result in material waste due to the removal of excess material. The proposed design features a shading structure that minimizes material usage while maintaining structural integrity. It also offers both aesthetic and functional advantages. This shading design can be easily fabricated using methods like 3D printing and can be validated easily. Advancements in 3D printing technology have enabled the fabrication of intricate shading designs, allowing for site-specific customization and large-scale production [22].

2.2. Shading System Design Framework

Figure 2 shows the framework that is used to help in designing the shading system. In the initial phase, a dataset is created through parametric simulations utilizing the Latin Hypercube Sampling (LHS) method, incorporating shading systems, design variables, and performance metrics. LHS is a statistical technique designed to efficiently generate diverse and representative samples of design variables, making it well-suited for complex computational models [42]. It minimizes the required sample size compared to random sampling, thereby decreasing the overall simulation time [43]. The dataset comprises values for design variables along with corresponding performance metrics. In the second stage within the MATLAB© version 2022b [44] environment, the generated dataset, consisting of design variable values and performance metrics, will be utilized to develop regression models for each performance measure using various machine learning algorithms, a process known as autoregression [8]. The auto regression utilizes different regression algorithms (artificial neural network (ANN), ensemble (ENS), decision tree (DT), and support vector machines (SVM)) that are optimized in a sequential way where the new regression algorithm is optimized to minimize the error and make it lower than the previous regression model. Combining different machine learning algorithms helps reduce overall regression time, as some models train faster than others, leading to a more efficient optimization process [8].

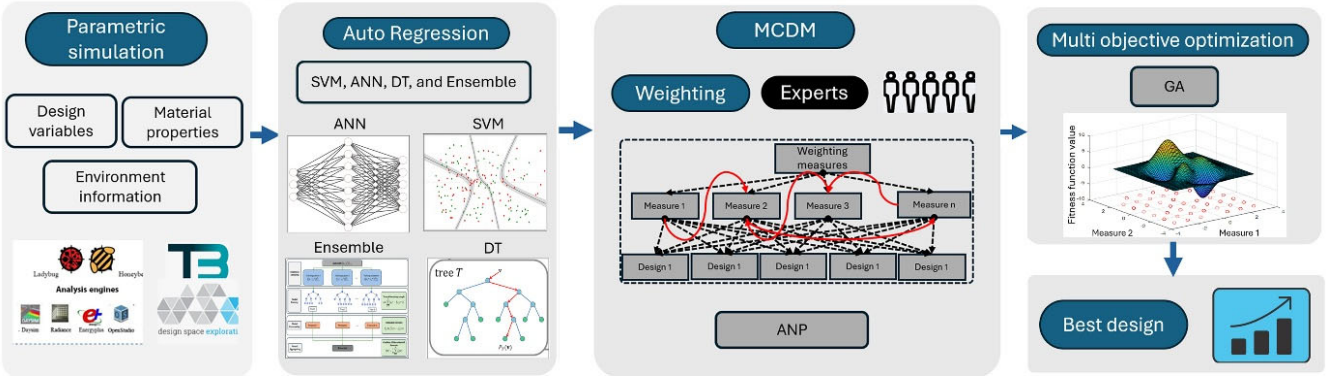

Figure 2. The framework of the proposed methodology.

After generating regression models, the regression models are combined into a single weighted fitness function. This combined fitness function is optimized using a widely adopted optimization algorithm (GA) [36,45]. The ANP method is used to weigh the performance measures. ANP is an extended version of the Analytic Hierarchy Process (AHP) that enables feedback and interactions between the performance measures [46,47]. After the GA optimization, the best design can be obtained easily.

2.3. Dataset Generation

The proposed algorithms will be applied to three different main case studies with different hot climate zones according to ASHRAE [48]. These main case studies include Cairo—Egypt, Riyadh—Saudi Arabia, and Kuching—Malaysia considering both south and west elevations. Detailed explanations of these main case studies are provided in the following sections.

2.3.1. Case Studies

The climate zoning and geographical information of the considered case studies are presented in Table 2. The selection of Cairo, Riyadh, and Kuching as case studies is based on their distinct climatic conditions, which present diverse challenges for daylighting and shading strategies. Cairo and Riyadh are examples of hot and very hot dry climates,

respectively, characterized by intense solar exposure. On the other hand, Kuching's tropical climate, with its very hot and humid conditions and predominance of diffuse daylight, poses unique challenges for designing energy-efficient daylighting systems. These variations provide a robust and comprehensive foundation for evaluating energy-efficient day lightening and shading solutions. The simulation is based on climate data from ref. [49], providing hourly recorded climate data of the city. Figure 3a shows the cumulative radiation coming from various directions in the selected cities. Overall, Cairo exhibits the most abundant radiation resources, followed by Riyad, while Kuching experiences the least radiation resources. Utilizing the concept of radiation advantages [50], we gain a profound understanding of the possible effects of radiation. Figure 3b presents the annual cumulative radiation benefit harm map, where the red color denotes negative values, and the green denotes positive values. It is apparent that in the three cities Solar radiation will mostly be harmful to the constructed thermal systems.

Table 2. Climatic zone, location, and the construction details for the considered case studies.

Representative City	Coordinate	Climate Zone	Construction	U-Factor ($W/(m^2 \cdot K)$)	Solar Heat Gain Coefficient
Cairo	30°7′19.2″ N, 31°24′21.6″ E	2B (hot dry)	Exterior wall with shading	0.760	N/A
			Other walls	Adiabatic	N/A
			Ground floor	2.014	N/A
			Window	2.57	0.25
Riyadh	24.7136° N, 46.6753° E	1B (very hot dry)	Exterior wall with shading	1.636	N/A
			Other walls	Adiabatic	N/A
			Ground floor	2.014	N/A
			Window	2.85	0.23
Kuching	1.5534° N, 110.3595° E	1A (Very hot humid)	Exterior wall with shading	1.636	N/A
			Other walls	Adiabatic	N/A
			Ground floor	2.014	N/A
			Window	2.85	0.23

Parametric modeling: The case study focuses on a single-zone workspace within a multi-story office building. The workspace has two key orientations: south and west, chosen for their energy and daylighting significance in hot climates. South-facing façades allow for controlled daylight entry and help reduce cooling demands. Meanwhile, west-facing façades require effective shading to address the intense heat and glare experienced in the afternoon. The façade is entirely glass-covered, which is recently used in office building in numerous countries to provide a modern aesthetic appeal [51,52], whereas the other façades have opaque elements. There are no artificial or natural obstructions in its surrounding context. The aim is to determine the effectiveness of the different shading devices on the cooling and the lighting [53]. The interior dimensions of the room are 4 m in height and 4 m in width, while the room depth is treated as a variable. The depth is considered within the range of 4 to 6 m [54]. This setup provides a controlled environment for analyzing the impact of design variations on workspace performance. As previously mentioned, the considered shading system is compared with the commonly used fins shading system [8,36,55,56]. The fins shading system is shown in Figure 4a and its design variables are shown in Figure 4b. The range of fins (vertical louvers) variables is determined based on studies conducted in hot regions [8,36,55,56]. These studies highlight that even within the same country, fins designs may need to be tailored to the specific latitude of each city [45]. Key factors such as the depth, number, and angle of fins have a significant impact on both visual comfort and energy performance. Additionally, the spacing between fins is an important consideration. The design variables and their ranges for each shading system and the building material optical properties can be seen in Table 3.

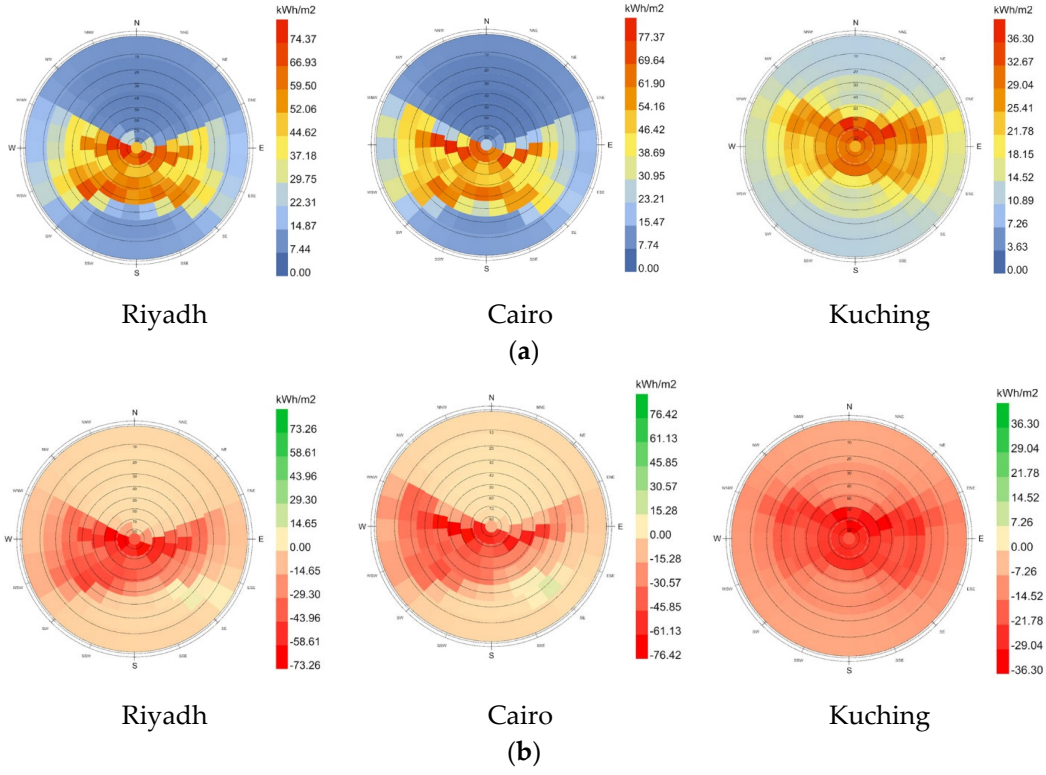

Figure 3. The annual cumulative radiation. (**a**) Annual sky cumulative radiation map; (**b**) Annual sky cumulative radiation benefit-harm map.

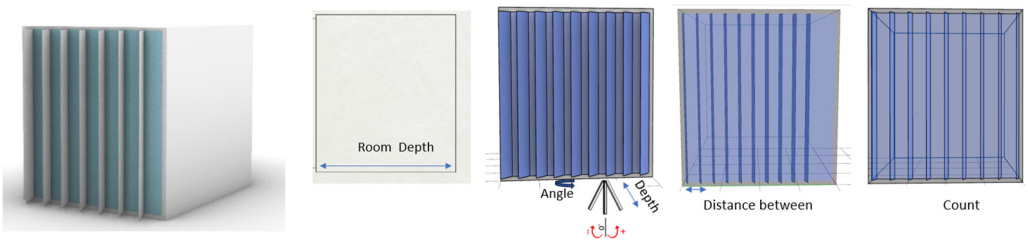

Figure 4. The considered fins shading system for comparison. (**a**) The 3D model. (**b**) The shading design variables.

Table 3. Design variables and their ranges and the building material optical properties.

Fins			PSS			Building Material Optical Properties		
Parameter	Range		Parameter	Range				
	Minimum	Maximum		Minimum	Maximum	Construction		Value
Room Depth	4 m	6 m	Room depth	4 m	6 m	Ceiling	reflectance	70%
Depth	0.2 m	0.4 m	Pattern depth	0.2 m	0.4 m	Floor	reflectance	20%
Angle	45°	−45°	Point coordinate (x)	0.1 m	1 m	Roof	reflectance	20%
Distance between	0.2 m	0.4 m	Point coordinate (y)	0.1 m	1 m	Wall	reflectance	50%
Count	5	10				Window	reflectance	0.6

Simulation performance: Parametric simulations for energy and daylight performance were conducted using Grasshopper components, specifically the Ladybug and Honeybee plugins (version 1.8), along with tools like EnergyPlus, OpenStudio, and Radiance/Daysim. The dataset was generated using Colibri, another Grasshopper plugin, to manage design parameters and collect simulation results. For daylight modeling, the building model was connected to Radiance materials with specified reflectance and transmittance values (Table 3), consistent across all three climate zones. The analysis grid comprised 255 points with a resolution of 0.25 m × 0.25 m at 0.8 m above the floor, based on an occupancy schedule from 9 AM to 5 PM. For energy modeling, the building model was linked to EnergyPlus materials, with thermal properties adapted for each city from ASHRAE Standard 90.1-2019 [57] (Table 2). To focus on shading performance, the ceiling, floor, and all walls (except the façade) were set as adiabatic, while an ideal air load system was used to manage cooling and heating set-point temperatures during occupied and unoccupied hours.

2.3.2. Performance Measures

This study examines five different performance measures, namely Useful Daylight Illuminance (UDI), Energy intensity use (EUI), Annual sun exposure (ASE), Continuous Daylight Autonomy (CDA), and Solar gains (SG). UDI: This metric represents the proportion of time spent within the effective occupancy period across three lighting ranges: 0–100 lux, 100–2000 lux, and above 2000 lux [58]. When daylight is 100–2000 lux, it is considered adequate natural light [59]. EUI: It is calculated using the annual energy consumption per square meter of the building, denoted in kWh/m^2 [60]. Annual consideration was given to the equipment load, artificial illumination load, cooling load, heating load, and equipment of the building. ASE: This metric is the percentage of analyzed space receiving more than a specified amount of direct sun radiation in a number of particular annual hours. The parameter was set to achieve (LEED) v4, and its value must not surpass 10% of floor area [61]. CDA: The CDA, refers to the proportion of time intervals throughout a year when the illuminance is above or below a certain value [62]. In this study, the value of the illuminance levels is 300 lux. SG: It is the total solar gain on any exterior surface, which is a combination of the absorption of direct and diffuse solar radiation [63].

2.4. Regression Models Generation

The dataset generated in the previous stage will be utilized to develop regression models for each of the performance metrics, including UDI, CDA, ASE, EUI, and SG. As we said earlier, the model selection process will involve optimizing the hyperparameters of four regression models in a successive way: ENS, DT, ANN, and SVM with the help of Bayesian optimization. The dataset is divided to 15% for testing, while training and validation are the rest. To minimize data overfitting, a 10-fold cross-validation method is applied. The evaluation metrics used are R^2 and MSE, which are standard measures for assessing the accuracy of machine learning models during both training and testing. It is calculated based on Equations (1) and (2) [64], respectively.

$$MSE = \frac{1}{N}\sum_{i=1}^{N}(\hat{y}_i - y_i)^2 \quad (1)$$

$$R^2 = 1 - \frac{\sum_{i=1}^{N}(\hat{y}_i - y_i)^2}{\sum_{i=1}^{N}(\hat{y}_i - y_i)^2} \quad (2)$$

where $\hat{y}_i$ is the expected illuminance for times i; y_i is the observed or simulated illuminance for times i : $\hat{y}_i$ is the average illuminance; and N is the number of data points evaluated.

2.5. Optimization

The regression models for the performance measures considered are combined in one weighted fitness function to be optimized. As we mentioned earlier, GA is used to optimize the objective function. The optimization problem can be mathematically expressed as follows:

$$\begin{aligned} minimize\ (S_1 \times w_1 \times Regression\ Model(x_1,\ x_2,\ \ldots,\ x_n) \\ +S_2 \times w_2 \times Regression\ Model(x_1,\ x_2,\ \ldots,\ x_n) + \ldots \\ +S_k \times w_k \times Regression\ Model(x_1,\ x_2,\ \ldots,\ x_n)) \end{aligned} \quad (3)$$

where X is the vector of the design variables $[x_1,\ x_2,\ x_3,\ \ldots,\ x_n]$, $i = 1,2,\ldots n$, n is the number of design variables, S is 1 for minimizing objectives and -1 for maximizing objectives, and k represents the number of objectives or performance measures being considered. The weights $(w_1,\ w_2,\ \ldots,\ w_k)$ that are employed in Equation (3), will be determined using ANP which will be explained in the following section.

2.6. MCDM—ANP

The steps of ANP are described as follows:

1. A group of experts will give their pairwise judgment (Analytic hierarchy process (AHP) pairwise comparison matrix) considering the relative importance of the performance measures using the popular Saaty's scale [65]. This scale is as follows: 1: Equal importance, 2: Weak importance, 3: Moderate importance, 4: Moderate plus, 5: Strong importance, 6: Strong plus, 7: Very strong importance, 8: Very very strong, 9: Extreme importance. The judging matrix (JM) is as follows:

$$JM_n = (m_{ij})_{k\times k} = \begin{bmatrix} m_{11} & m_{12} & \ldots & m_{1k} \\ m_{21} & m_{22} & \ldots & m_{2k} \\ \vdots & \vdots & \ddots & \vdots \\ m_{k1} & m_{k2} & \ldots & m_{kk} \end{bmatrix} \quad (4)$$

where $m_{ij} \geq 0$, $m_{ij} = 1/m_{ji}$, and k is the number of performance measures and n is the expert index.

2. For each of these matrices, the cumulative column product is calculated then the weight vector w_k, which is the geometric mean of the resulting values, which is then normalized by dividing w_k to the summation of the vector.
3. Then, the consistency index CI, random consistency RC, and consistency ratio CR are calculated. Where $CR = CI/RC$, the consistency index is accepted only if $CR \leq 0.1$.
4. Subsequently, the opinion of each expert will be obtained as a weight vector W_n for each performance measure.
5. The weight vector W_n that is obtained in AHP will be employed in ANP.
6. Interdependence among the criteria is addressed by conducting pairwise comparisons (IJM) to assess the impact of each criterion on the others, with input provided by experts.

$$IJM_n = (dm_{ij})_{k\times k} = \begin{bmatrix} dm_{11} & dm_{12} & \ldots & dm_{1k} \\ dm_{21} & dm_{22} & \ldots & dm_{2k} \\ \vdots & \vdots & \ddots & \vdots \\ dm_{k1} & dm_{k2} & \ldots & dm_{kk} \end{bmatrix} \quad (5)$$

where $0 \leq dm_{ij} \geq 1$, 0 means no interdependence and 1 means full interdependence.

7. Then, the normalized matrix ($NIJM$) is calculated based on the following equation:

$$NIJM_n = \left(ndm_{ij}\right)_{k\times k} \tag{6}$$

$$ndm_{ij} = \frac{dm_{ij}}{\sum_{i=1}^{k} dm_{ij}} \tag{7}$$

8. Then, the adjusted weight vector AW_n are calculated as follows:

$$AW_n = NIJM_n \times W_n \tag{8}$$

9. Then, those weights will be combined in a single weight vector through taking the arithmetic means.

For more details on the ANP and AHP method, please refer to refs. [47,66].

3. Results and Discussion

A total of 2000 simulations for each city were conducted on the Honeybee for Grasshopper platform for training the machine learning models. Table 4 shows the type of regression models and the corresponding MSE and R^2 values acquired through the application of the generated models to the testing datasets pertaining to the south and west elevations for the cities considered. The regression models achieved good R^2 and MSE testing values. These regression models will be used in the optimization function as explained in the optimization section.

Table 4. The obtained regression model for each case study and the corresponding MSE and R^2.

Case	Metric	Regression Model	MSE	R^2	Case	Metric	Regression Model	MSE	R^2
Fins Cairo South	ASE	ANN	1.4	0.98	Fins Cairo West	ASE	SVM	0.17	0.85
	CDA	ANN	0.03	0.99		CDA	Ensemble	0.03	0.97
	EUI	SVM	1.8	0.95		EUI	ANN	1.57	0.98
	SG	Ensemble	1.5	0.94		SG	Ensemble	1.6	0.93
	UDI	ANN	0.04	0.99		UDI	Ensemble	0.04	0.99
PSS Cairo South	ASE	Ensemble	1.6	0.99	PSS Cairo West	ASE	Ensemble	1.22	0.99
	CDA	Ensemble	0.035	0.98		CDA	Ensemble	0.04	0.97
	EUI	Ensemble	1.14	0.98		EUI	Ensemble	1.25	0.99
	SG	SVM	0.005	0.05		SG	Ensemble	0.005	0.99
	UDI	Ensemble	0.05	0.99		UDI	Ensemble	0.024	0.99
Fins Kuching South	ASE	Ensemble	1.29	0.99	Fins Kuching West	ASE	ANN	1.8	0.97
	CDA	SVM	0.037	0.97		CDA	SVM	0.037	0.99
	EUI	Ensemble	1.5	0.8		EUI	SVM	1.4	0.92
	SG	Ensemble	1.02	0.83		SG	Ensemble	1.4	0.91
	UDI	ANN	0.041	0.94		UDI	ANN	0.041	0.99
PSS Kuching South	ASE	Ensemble	0.85	0.96	PSS Kuching West	ASE	Ensemble	1.13	0.99
	CDA	SVM	0.037	0.99		CDA	ANN	0.037	0.99
	EUI	ANN	1.8	0.99		EUI	ANN	1.7	0.88
	SG	Ensemble	1.09	0.99		SG	Ensemble	1.9	0.99
	UDI	ANN	0.041	0.99		UDI	Ensemble	0.04	0.99
Fins Riyadh South	ASE	ANN	1.23	0.98	Fins Riyadh West	ASE	Ensemble	1.5	0.86
	CDA	ANN	0.003	0.96		CDA	ANN	0.37	0.91
	EUI	ANN	1.6	0.98		EUI	ANN	1.2	0.94
	SG	Ensemble	1.13	0.93		SG	Ensemble	1.6	0.81
	UDI	ANN	0.07	0.99		UDI	ANN	0.5	0.93
PSS Riyadh South	ASE	Ensemble	1.2	0.99	PSS Riyadh West	ASE	Ensemble	1.8	0.99
	CDA	SVM	0.08	0.98		CDA	SVM	0.04	0.98
	EUI	SVM	0.06	0.99		EUI	SVM	0.27	0.99
	SG	Ensemble	1.7	0.99		SG	Ensemble	1.6	0.99
	UDI	ANN	0.026	0.99		UDI	ANN	0.028	0.99

3.1. MCDM

Eight experts will rank the importance of the five metrics using the AHP pairwise comparison matrix and put a score that indicates the interdependence between the performance measures. The AHP matrices can be seen in Figure 5a. These matrices will be used to obtain the weights of each performance measure for ANP, which can be seen in Figure 5b. We obtained the weights from both AHP and ANP to show that considering the interdependency between the performance measures can affect the final weights of the performance measures. Specifically, this adjustment reduces the weights assigned to UDI and EUI while increasing the weights for CDA, solar gains, and ASE.

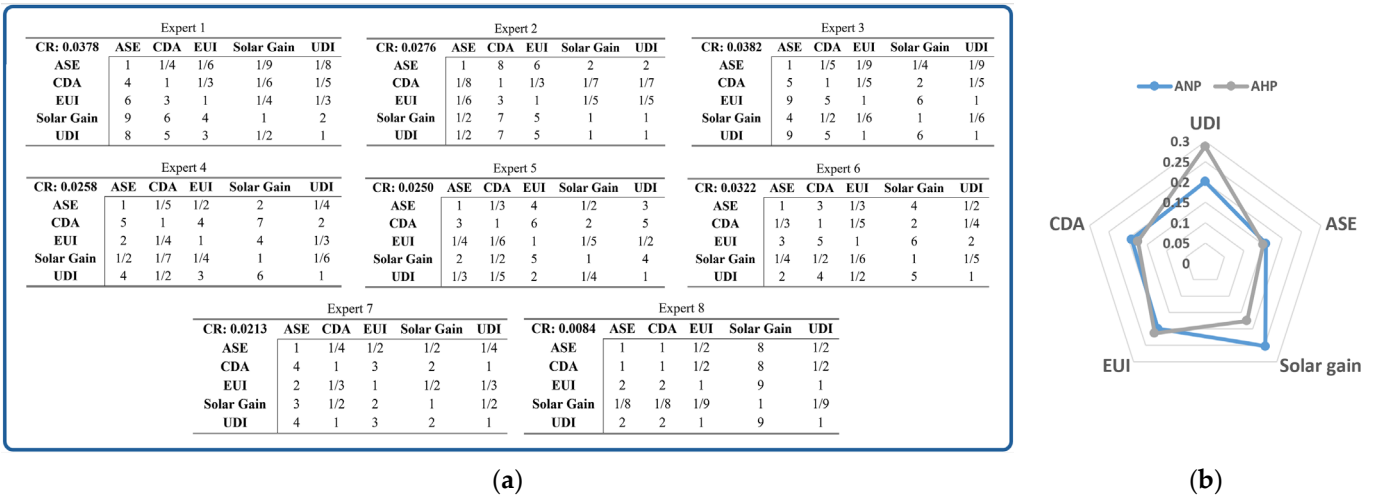

Expert 1

CR: 0.0378	ASE	CDA	EUI	Solar Gain	UDI
ASE	1	1/4	1/6	1/9	1/8
CDA	4	1	1/3	1/6	1/5
EUI	6	3	1	1/4	1/3
Solar Gain	9	6	4	1	2
UDI	8	5	3	1/2	1

Expert 2

CR: 0.0276	ASE	CDA	EUI	Solar Gain	UDI
ASE	1	8	6	2	2
CDA	1/8	1	1/3	1/7	1/7
EUI	1/6	3	1	1/5	1/5
Solar Gain	1/2	7	5	1	1
UDI	1/2	7	5	1	1

Expert 3

CR: 0.0382	ASE	CDA	EUI	Solar Gain	UDI
ASE	1	1/5	1/9	1/4	1/9
CDA	5	1	1/5	2	1/5
EUI	9	5	1	6	1
Solar Gain	4	1/2	1/6	1	1/6
UDI	9	5	1	6	1

Expert 4

CR: 0.0258	ASE	CDA	EUI	Solar Gain	UDI
ASE	1	1/5	1/2	2	1/4
CDA	5	1	4	7	2
EUI	2	1/4	1	4	1/3
Solar Gain	1/2	1/7	1/4	1	1/6
UDI	4	1/2	3	6	1

Expert 5

CR: 0.0250	ASE	CDA	EUI	Solar Gain	UDI
ASE	1	1/3	4	1/2	3
CDA	3	1	6	2	5
EUI	1/4	1/6	1	1/5	1/2
Solar Gain	2	1/2	5	1	4
UDI	1/3	1/5	2	1/4	1

Expert 6

CR: 0.0322	ASE	CDA	EUI	Solar Gain	UDI
ASE	1	3	1/3	4	1/2
CDA	1/3	1	1/5	2	1/4
EUI	3	5	1	6	2
Solar Gain	1/4	1/2	1/6	1	1/5
UDI	2	4	1/2	5	1

Expert 7

CR: 0.0213	ASE	CDA	EUI	Solar Gain	UDI
ASE	1	1/4	1/2	1/2	1/4
CDA	4	1	3	2	1
EUI	2	1/3	1	1/2	1/3
Solar Gain	3	1/2	2	1	1/2
UDI	4	1	3	2	1

Expert 8

CR: 0.0084	ASE	CDA	EUI	Solar Gain	UDI
ASE	1	1	1/2	8	1/2
CDA	1	1	1/2	8	1/2
EUI	2	2	1	9	1
Solar Gain	1/8	1/8	1/9	1	1/9
UDI	2	2	1	9	1

(**a**) (**b**)

Figure 5. Weighting results. (**a**) The AHP pairwise comparison matrices. (**b**) The weights of objectives using AHP and ANP.

3.2. Analysis

The performance improvements (with respect to the design without shading) for the best obtained designs for both fins and PSS systems can be seen in Figure 6. In the case of Egypt–Cairo, the best PSS design achieved, increasing UDI by 57.7% and CDA by 7.3%, compared to 21% and 0.82% for fins. Additionally, PSS reduced ASE, SG, and EUI by 97.12%, 75.7%, and 31.7%, respectively, while fins achieved reductions of 5.8%, 42.3%, and 16.4%. For the south elevations, PSS showed an increase in UDI (59.19%) and CDA (8.1%), compared to 25.2% and 1.3% for the fins. PSS also achieved a reduction in ASE (99.68%), SG (85.6%), and EUI (45.2%) compared to fins, which reduced ASE by 21.62%, SG by 75.9%, and EUI by 34.4%.

In the case of Malaysia–Kuching with west elevations, PSS showed significant improvements by, increasing UDI by 93.6% and CDA by 9.6%, compared to 35.6% and 1.4% for fins. PSS also achieved a reduction in ASE, SG, and EUI, with reductions of 100%, 82.69%, and 13.78%, respectively, compared to fins' reductions of 25.9%, 42.46%, and 10.1%. For the south elevations, PSS increased UDI by 105.32% and CDA by 9.14%, while fins showed only a 17.2% increase in UDI and 1.3% in CDA. Additionally, PSS achieved larger reductions in ASE (100%), SG (82.3%), and EUI (41.94%), and fins reduced ASE by 31.1%, SG by 38.1%, and EUI by 12.4%.

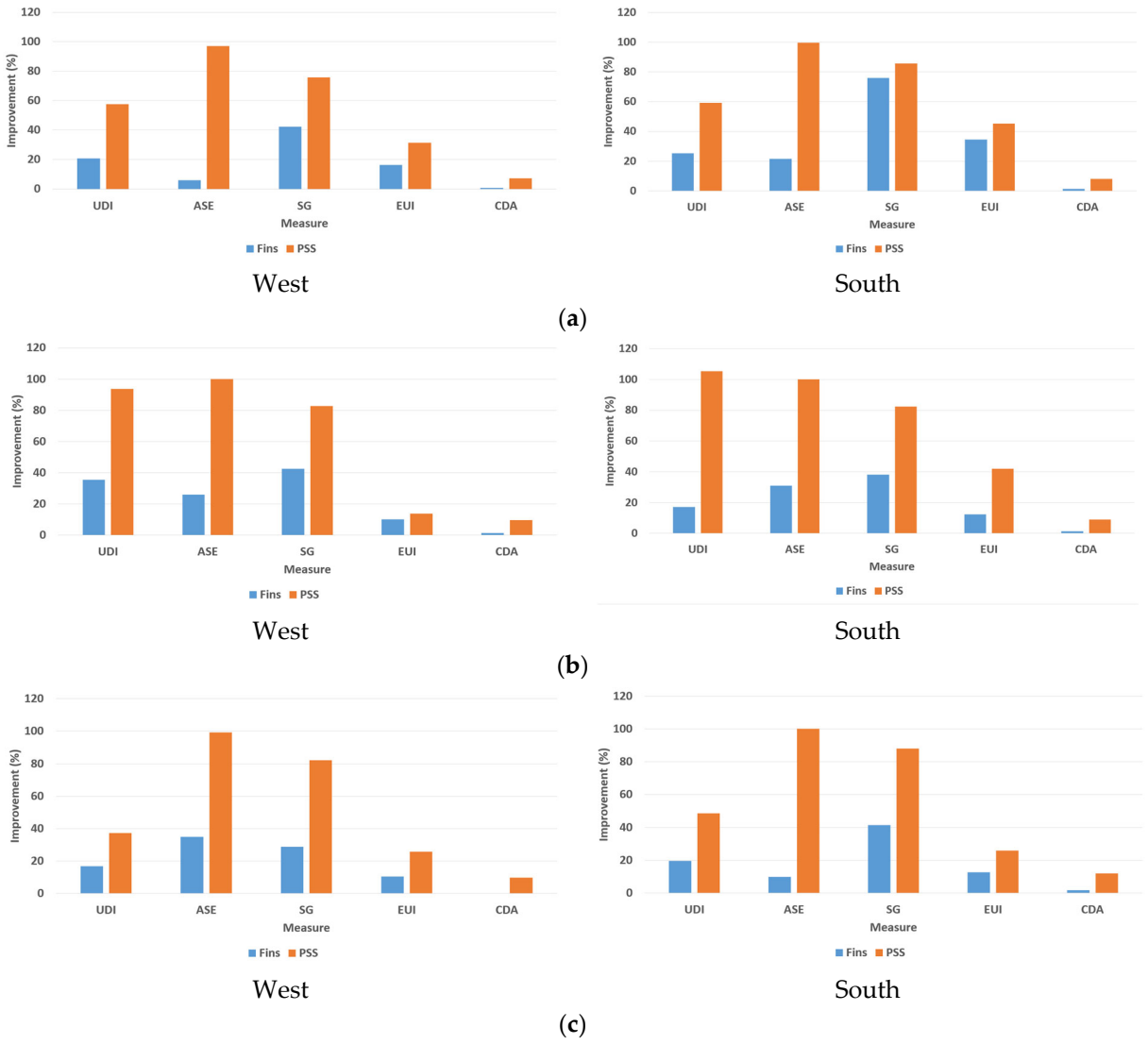

Figure 6. Improvement in each performance measure for the fins and the proposed PSS shading system: (**a**) Cairo; (**b**) Kuching; (**c**) Riyadh.

In the case of Saudi Arabia–Riyadh, for the west elevations, PSS outperformed fins by increasing UDI by 37.62% and CDA by 9.67%, compared to fins' increases of 16.7% and 0.13%, respectively. PSS also achieved greater reductions in ASE, SG, and EUI, with reductions of 99.24%, 82.16%, and 25.62%, respectively, while fins reduced these measures by 36.82%, 28.8%, and 10.36%. For the south elevations, PSS showed a significant increase in UDI (48.68%) and CDA (11.87%) compared to fins, which achieved only 19.5% and 1.6%, respectively. PSS also outperformed fins in reducing ASE (100%), SG (88.07%), and EUI (25.89%), while fins reduced ASE by 9.9%, SG by 41.38%, and EUI by 12.64%.

The proposed PSS consistently performed better than traditional fins on both south and west-facing elevations. The proposed PSS shows varying results in the case studies of Cairo, Kuching, and Riyadh due to differences in climatic conditions, solar exposure, and daylight availability, as detailed in the case studies section. These factors affect the performance measures, leading to different design solutions tailored to each climate. The hybrid design system adapts to the circumstances of each location, ensuring the best performance for the particular environmental conditions of Cairo, Kuching, and Riyadh. The hybrid approach provides a systematic and comprehensive method for identifying the optimal design by considering all relevant design aspects. Moreover, its versatility allows it to be applied to

various shading systems, as demonstrated in its successful application to both perforated shading screens (PSS) and vertical fins. This adaptability makes it a valuable tool for optimizing different shading strategies across diverse architectural contexts. Figure 7a presents the best PSS designs for each city, while Figure 7b displays a 3D-printed model of the optimum PSS design for Egypt's south elevation.

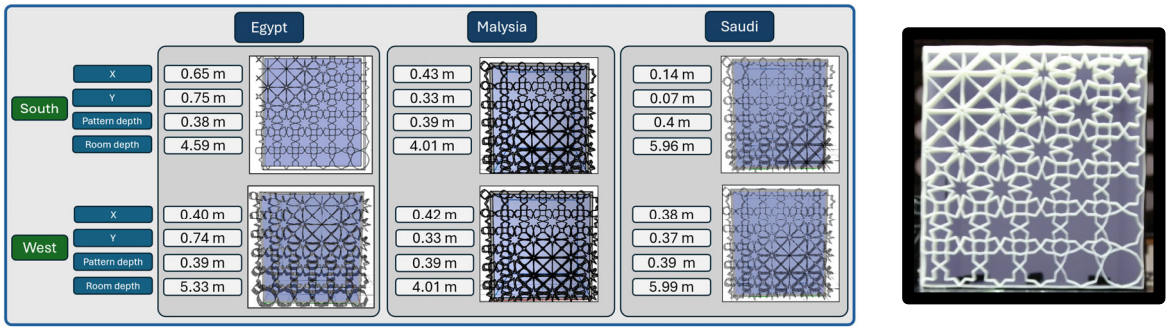

(**a**) (**b**)

Figure 7. The obtained optimum PSS designs: (**a**) The best PSS designs obtained for each case study; (**b**) One of the 3D printed PSS.

3.3. Experimental Validation of the PSS Shading System

This experiment is conducted to evaluate and validate the performance of the PSS, focusing on the best PSS design obtained for Egypt-south to simplify the analysis. This experiment studies the visual effects on the occupants under various daylight conditions using 15 standard sky (15 CIE). This is accomplished via the sky dome depicted in Figure 8.

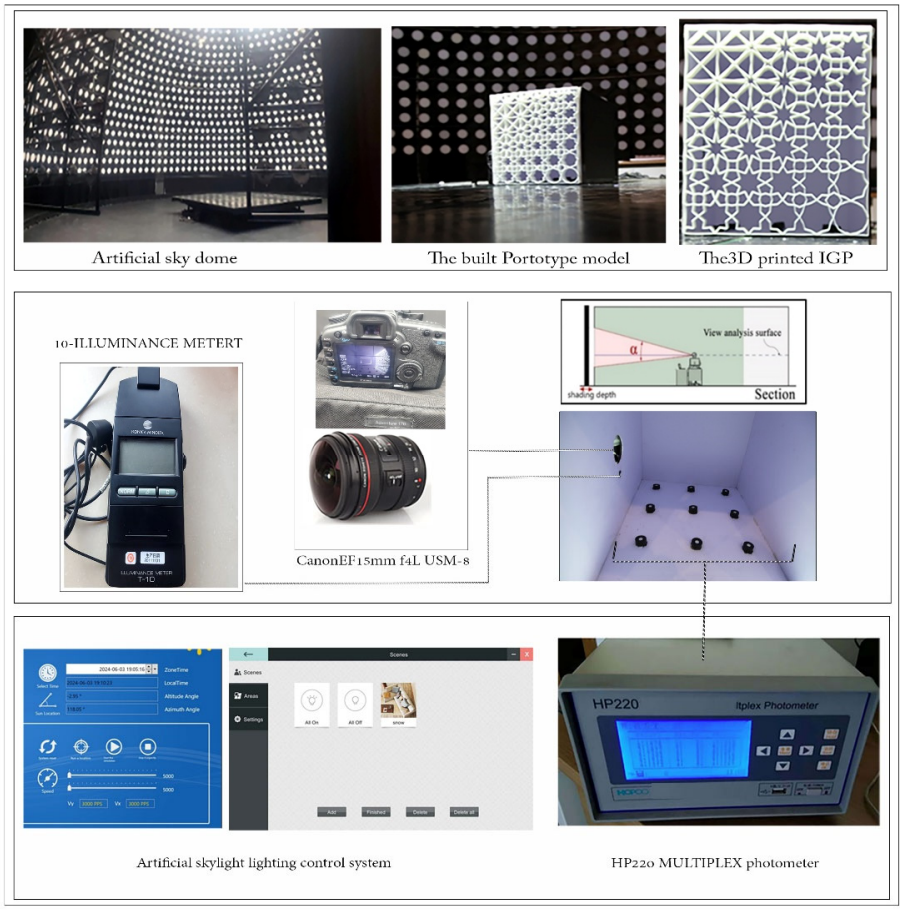

Figure 8. Experimental setup for the validation of the PSS shading system.

The optimized shading design's effectiveness can be verified by re-evaluating it under 15 CIE sky conditions, ensuring it effectively manages daylight and glare, consistently providing visual comfort, confirming the desired outcomes in real-world conditions. This approach saves a lot of time and avoids the complexities associated with using a real sky model. These 15 sky types are as follows:

(1) ClE standard overcast sky, steep luminance gradation towards zenith, azimuthal uniformity.
(2) Overcast, with steep luminance gradation and slight brightening towards the sun.
(3) Overcast, moderately graded with azimuthal uniformity.
(4) Overcast, moderately graded and slightly brightening towards the sun.
(5) Sky of uniform luminance.
(6) Partly cloudy sky, no gradation towards zenith, slight brightening towards the sun.
(7) Partly cloudy sky, no gradation towards zenith, brighter circumsolar region.
(8) Partly cloudy sky, no gradation towards zenith, distinct solar corona.
(9) Partly cloudy, with the obscured sun.
(10) Partly cloudy, with brighter circumsolar region.
(11) White-blue sky with distinct solar corona.
(12) ClE standard clear sky, low luminance turbidity.
(13) ClE standard clear sky, polluted atmosphere.
(14) Cloudless, turbid sky with broad solar corona.
(15) White-blue turbid sky with broad solar corona.

The luminance fluctuates continuously for all sky standards, and the distribution patterns can be defined by simple mathematical equations and it can be reviewed at [67,68]. Two daylight indicators are considered for the evaluation: The illumination uniformity (Uniformity) [69,70], and daylight glare probability (DGP) (for predicting indoor glare [71]) using Evaglare [72]. These indicators are calculated as follows:

$$\text{Uniformity} = \frac{E_{min}}{E_{avg}} \tag{9}$$

$$DGP = 5.87 \times 10^{-5} E_v + 9.18 \times 10^{-5} log_{10} 2(1 + \sum_{i=1}^{n} \frac{L_{s,i}\omega_{s,i}}{E_v^{1.87} P_i^2}) + 0.16 \tag{10}$$

where uniformity is the illumination uniformity index, E_{min} is the minimum illuminance, on the specified surface, and E_{avg} is the average illuminance on the specified surface. E_v is the vertical illuminance. L_s is the luminance of the source (cd/m^2), ω_s solid angle of the i-th glare source based on the viewing position of the observer, P_i and is position index of the i-th glare source.

The model was built with 1:10 scale with respect to the best design obtained as shown in Figure 8. The experiment was conducted in the sky model (see Figure 8) in the artificial sky laboratory, which consists of 29 rings of translucent diffusing luminaires, evenly distributed within the dome. The elevation angles range from 1.2° to 82.66°. Three photometric instruments were used to 'instantaneously' capture the luminous environment of the observer (see Figure 8). Horizontal illuminance is measured using the HP200 multiplex photometer with ±4% accuracy. Measurements are taken at 13 points—12 inside and 1 outside the model. The average illuminance and uniformity are determined using the average and minimum values of the 12 interior points. A Canon EOS 5D Mark II with a fisheye lens is used to measure luminance distribution, positioned at eye height (1.30 m, or 13 cm in the model). The camera operates in manual exposure mode, capturing Low Dynamic Range (LDR) images with various exposure values (1/8000 to 5 s). These are combined into a High Dynamic Range (HDR) image using Picture Naut and HDR Scope software version 1 [73,74]. The process includes vignetting and luminance correction (see

Figure 9), followed by calculating the indoor glare predictor (DGP). The T10-M vertical luminance meter, with a measurement range of 0.01 lx to 2999 klx and ±1% accuracy, is used for calibrating HDR image brightness and measuring vertical illuminance.

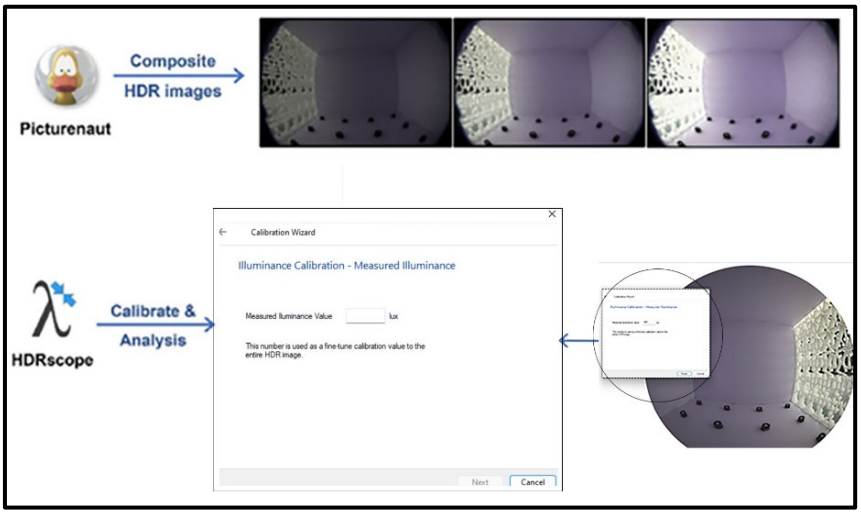

Figure 9. Combining and evaluating the HDR images.

The performance of the PSS system was evaluated under all 15 CIE Standard Sky models, with a focus on two key metrics: illumination uniformity index and daylight glare probability (DGP). The findings are presented in Figures 10 and 11 and are discussed in detail below.

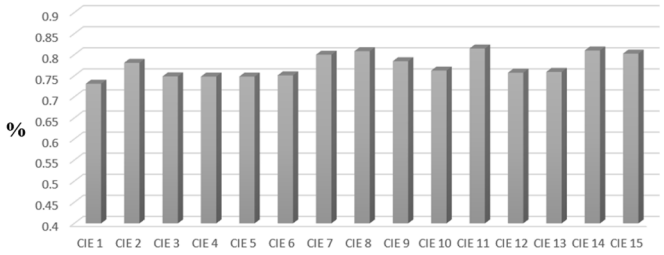

(**a**)

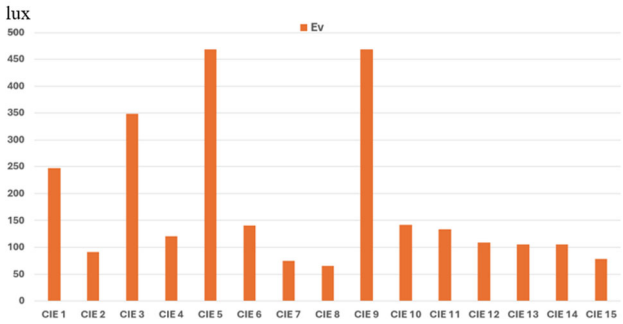

(**b**)

Figure 10. Experiment results (**a**) illumination uniformity (**b**) Ev values under 15 skies.

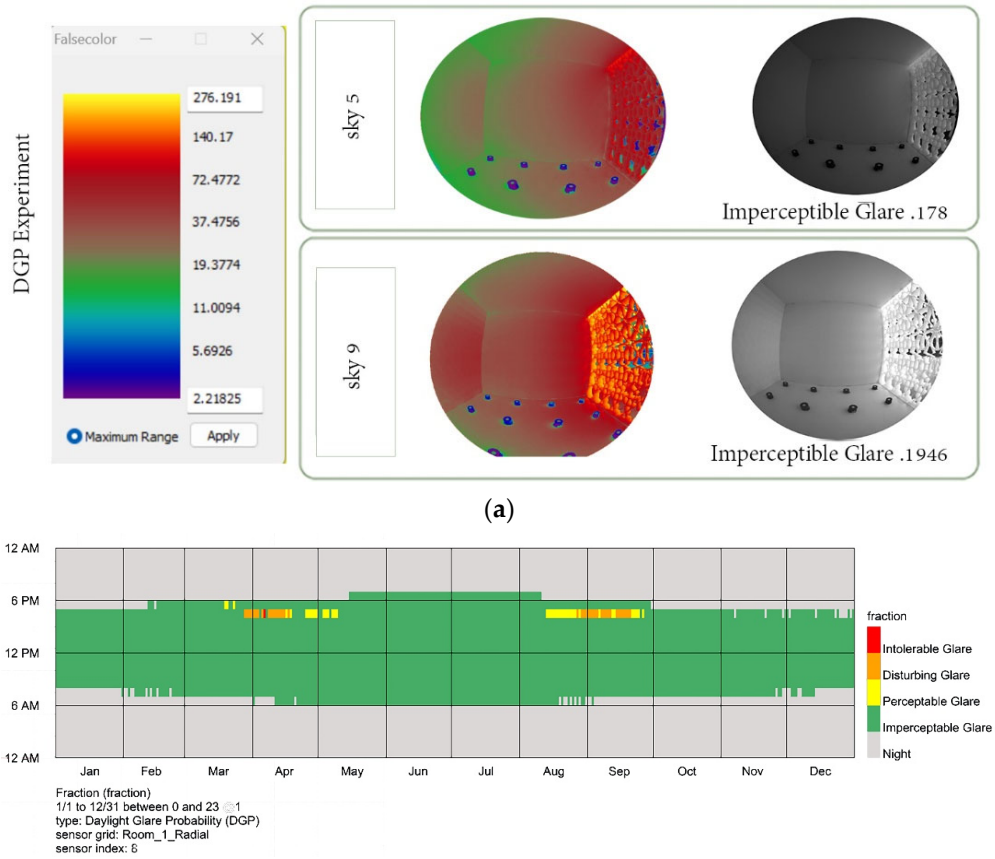

Figure 11. Daylight glare probability. (**a**) color false image with DGP results. (**b**) Grasshopper glare results.

Illumination Uniformity Index: The illumination uniformity index was calculated for all 15 sky models to assess the effectiveness of the shading system in achieving consistent daylight distribution, which is shown in Figure 10. According to ref. [70], a uniformity index value above 0.6 is considered acceptable for shading systems. In this study, all sky models demonstrated uniformity values exceeding 0.7, indicating a high level of daylight uniformity across varying sky conditions, especially for skies 7, 8, 11, 14, and 15. This result confirms that the PSS system effectively distributes daylight, ensuring optimal visual comfort and performance under diverse environmental scenarios.

Daylight Glare Probability: To evaluate the potential for glare, the daylight glare probability (DGP) was analyzed for the sky models with the highest illuminance values (Ev). Among the 15 sky models, Sky 5 and Sky 9 exhibited the highest Ev values, suggesting a greater likelihood of glare occurrence. The DGP calculations for these two sky models revealed an "imperceptible" glare rating, as illustrated in Figure 11. This outcome underscores the effectiveness of the PSS system in mitigating glare, even under the most challenging sky conditions.

The physical testing results align closely with the outcomes of the Grasshopper simulation model, which also predicted an imperceptible glare level for the optimal shading design. This consistency between physical and simulation data validates the accuracy and reliability of the computational model, reinforcing its utility for future design and optimization of shading systems.

3.4. Summary of the Main Findings

This study demonstrated the effectiveness of the proposed PSS in improving daylight performance and energy efficiency across three climatic regions: Cairo (Egypt), Kuching (Malaysia), and Riyadh (Saudi Arabia). The results showed that the PSS consistently outperformed traditional fins by enhancing UDI and CDA, while significantly reducing ASE, SG, and EUI. Kuching exhibited the highest increase in UDI (105.32%), while Riyadh showed the highest CDA improvement (11.87%). The PSS also achieved notable reductions in EUI, particularly in Cairo (45.2%) and Kuching (41.94%), highlighting its potential to optimize energy consumption in hot climates. Experimental validation confirmed the PSS's ability to provide high illumination uniformity and imperceptible glare levels even under extreme daylight conditions, aligning with simulation predictions. The integration of the ANP allowed for an optimized shading design, balancing multiple performance metrics and considering their interdependence.

The findings of this study contribute to the existing literature by expanding the scope of shading system evaluation beyond the common focus on south-facing orientations. By evaluating both south and west elevations, the research provides a broader perspective on shading performance under different solar conditions. While many studies rely on simulations alone, this research integrates experimental validation, confirming the real-world effectiveness of the PSS. The use of the ANP enables a more comprehensive and realistic optimization, accounting for the interactions between daylighting, glare control, and energy efficiency, which is often overlooked in previous studies. This approach positions the PSS as a high-performance and adaptable solution, suitable for a variety of climates.

The implications of these findings are significant for the future design and adoption of sun-shading systems. The study emphasizes the value of culturally inspired, perforated designs that balance aesthetic appeal with functional performance, suggesting that shading systems can be both visually pleasing and efficient. The proposed PSS effectively reduces solar glare and energy consumption while enhancing daylight performance, encouraging architects and engineers to explore similar innovative solutions. Its adaptability to different climates, particularly regions with high solar exposure and humidity, makes it a promising solution for diverse architectural contexts. By bridging the gap between simulation-based optimization and real-world applications, this research provides a data-driven framework for the development of more sustainable, adaptive, and efficient sun-shading strategies in architecture.

3.5. Limitations and Future Work

While the proposed shading system demonstrates promising results, the study is based on simulations and controlled experiments, which may not fully reflect existing building conditions. Factors such as varying building orientations, occupant behavior, and shading material types were not considered. Future research will address these limitations by conducting tests on an existing building. Additionally, exploring the impact of different materials on the proposed PSS's durability, cost, and environmental impact would be beneficial. Expanding the study to include temperate and cold climates will help assess the system's versatility across diverse environmental conditions, enhancing its practical relevance and contributing to the development of more sustainable shading solutions.

4. Conclusions

The proposed PSS-star pattern system that is inspired by the traditional Middle Eastern Mashrabiya style consistently surpasses the traditional fins system, delivering significant enhancements in both daylighting and energy performance in all case studies

(Cairo, Kuching, and Riyadh) for both south and west-facing elevations. Using the hybrid design approach, different PSS design is obtained for each case study offering different performance and results for each case study. This is due to the variations in climatic conditions, solar exposure, and daylight availability. In hot, arid climates like Cairo (hot dry) and Riyadh (very hot dry), characterized by intense solar radiation and high temperatures, the optimal PSS design significantly reduced glare and energy use while enhancing daylight autonomy. In Cairo, UDI increased by up to 59.19%, CDA by 8.1%, while ASE, SG, and EUI were reduced by 99.68%, 85.6%, and 45.2%, respectively. In Riyadh, UDI improved by 48.68%, CDA by 11.87%, with ASE nearly eliminated (99.24–100% reduction), SG reduced by 88.07%, and EUI lowered by 25.89%. In the tropical climate of Kuching (Very hot humid), which experiences high humidity and diffuse daylight, the optimal PSS design PSS maximized daylight penetration and eliminated excessive solar exposure. Increasing UDI by up to 105.32% and CDA by 9.6%, while completely eliminating ASE (100% reduction). SG and EUI also saw significant decreases of 82.3% and 41.94%. The results indicate that the proposed PSS is highly adaptable to different climatic conditions, effectively improving daylight performance and reducing energy consumption across diverse environments. These findings suggest that climate-specific shading designs are essential for optimizing performance and that the hybrid design successfully tailors PSS configurations to varying environmental demands. The proposed PSS system is most beneficial in tropical climates, such as Kuching, Malaysia, where it achieved the highest improvements in UDI and completely eliminated ASE, while also significantly reducing SG and EUI. In contrast, PSS is least beneficial in hot desert climates, such as Riyadh, Saudi Arabia, where although it still provides substantial improvements, it can effectively reduce glare and overheating. The design framework effectively manages design complexities, conflicting metrics, interdependencies, and architects' preferences. It applies to both simple and complex shading systems, ensuring optimal solutions. Results showed that considering interdependencies influences metric weights, impacting final design selection. A 3D printed model of the optimal shading design for one of the case studies is experimentally validated and tested under 15 standard sky conditions to evaluate its impact on occupants. This result confirms that the PSS system effectively distributes daylight, ensuring optimal visual comfort and performance under diverse environmental scenarios, especially for skies 7, 8, 11, 14, and 15, which achieved the highest illumination uniformity and low glare probability. The results also showed the effectiveness of the PSS system in mitigating glare, even under the most challenging sky conditions (Sky 5: sky of uniform luminance and Sky 9: partially cloud with the obscured sun), which has the highest illuminance values (Ev). Future research should focus on testing the proposed shading systems (PSS) in existing buildings to evaluate their performance under actual conditions, while also investigating the impact of different materials and cost factors to determine economic feasibility and durability.

Author Contributions: Conceptualization, B.G.; methodology, B.G. and M.O.; software, M.O.; validation, B.G.; formal analysis, B.G. and M.O.; investigation, B.G. and M.O.; resources, C.Z. and X.H.; data curation, B.G.; writing—original draft preparation, B.G. and M.O.; writing—review and editing, B.G., C.Z., X.H., M.O. and G.L.; visualization, B.G.; supervision, C.Z. and X.H.; project administration, C.Z. and G.L.; funding acquisition, C.Z. and G.L. All authors have read and agreed to the published version of the manuscript.

Funding: This research has been funded by the National Natural Science Foundation of China (No. 51778168 and No. 52278054).

Data Availability Statement: The raw data supporting the conclusions of this article will be made available by the authors on request.

Conflicts of Interest: The authors declare no conflicts of interest.

Abbreviations

PSS	Perforated shading screen
MCDM	Multi-criteria decision-making
GA	Genetic algorithm
ANP	Analytic Network Process
ANN	Artificial neural networks
MAUT	Multi-Attribute Utility Theory
UDI	Useful Daylight Illuminance
EUI	Energy intensity use
ASE	Annual sun exposure
CDA	Continuous Daylight Autonomy
SG	Solar gains
LHS	Latin hypercube sampling method
ENS	Ensemble
DT	Decision tree
SVM	Support vector machines
AHP	Analytic Hierarchy Process

References

1. Kamal, A.; Kadam, S.T.; Hou, D.; Hassan, I.G.; Wang, L.; Sezer, N.; Rahman, M.A. Detailed profiling of high-rise building energy consumption in extremely hot and humid climate. *Clean. Energy Syst.* **2023**, *4*, 100060. [CrossRef]
2. Lakhdari, K.; Sriti, L.; Painter, B. Parametric optimization of daylight, thermal and energy performance of middle school classrooms, case of hot and dry regions. *Build. Environ.* **2021**, *204*, 108173. [CrossRef]
3. Mahrous, R.; Giancola, E.; Osman, A.; Asawa, T.; Mahmoud, H. Review of key factors that affect the implementation of bio-receptive façades in a hot arid climate: Case study north Egypt. *Build. Environ.* **2022**, *214*, 108920. [CrossRef]
4. Ishac, M.; Nadim, W. Standardization of optimization methodology of daylighting and shading strategy: A case study of an architectural design studio—The German University in Cairo, Egypt. *J. Build. Perform. Simul.* **2021**, *14*, 52–77. [CrossRef]
5. Rocha, A.P.d.A.; Oliveira, R.C.L.F.; Mendes, N. Technical Review of Solar Distribution Calculation Methods: Enhancing Simulation Accuracy for High-Performance and Sustainable Buildings. *Buildings* **2025**, *15*, 578. [CrossRef]
6. Yusoff, W.F.M.; Shaharil, M.I.; Mohamed, M.F.; Rasani, M.R.M.; Sapian, A.R.; Dahlan, N.D. Review of openings with shading devices at naturally ventilated buildings. *Archit. Eng. Des. Manag.* **2023**, *19*, 463–479. [CrossRef]
7. Masoud, S.; Zamani, Z.; Hosseini, S.M.; Attia, S. A Review of Factors Affecting the Lighting Performance of Light Shelves and Controlling Solar Heat Gain. *Buildings* **2024**, *14*, 1832. [CrossRef]
8. Gaber, B.; Zhan, C.; Han, X.; Omar, M.; Li, G. A novel decision support system for designing fixed shading systems in the early design stage: A case study in Egypt. *J. Build. Eng.* **2024**, *96*, 110453. [CrossRef]
9. Koç, S.G.; Maçka Kalfa, S. The effects of shading devices on office building energy performance in Mediterranean climate regions. *J. Build. Eng.* **2021**, *44*, 102653. [CrossRef]
10. Al-Saadi, S.N.; Al-Jabri, K.S. Optimization of envelope design for housing in hot climates using a genetic algorithm (GA) computational approach. *J. Build. Eng.* **2020**, *32*, 101712. [CrossRef]
11. Al-Kodmany, K. Sustainability and the 21st Century Vertical City: A Review of Design Approaches of Tall Buildings. *Buildings* **2018**, *8*, 102. [CrossRef]
12. Lumpkin, D.R.; Horton, W.T.; Sinfield, J.V. Holistic synergy analysis for building subsystem performance and innovation opportunities. *Build. Environ.* **2020**, *178*, 106908. [CrossRef]
13. Huang, L.; Zou, K.; Zhang, X.; Zhao, S. Effects of non-uniform perforated solar screen on daylighting and visual comfort performance. *J. Build. Eng.* **2024**, *97*, 110684. [CrossRef]
14. Chi, D.A.; Moreno, D.; Navarro, J. Design optimisation of perforated solar façades in order to balance daylighting with thermal performance. *Build. Environ.* **2017**, *125*, 383–400. [CrossRef]
15. Fernando, D.; Navaratnam, S.; Rajeev, P.; Sanjayan, J. Study of Technological Advancement and Challenges of Façade System for Sustainable Building: Current Design Practice. *Sustainability* **2023**, *15*, 14319. [CrossRef]
16. Caetano, I.; Leitão, A. Mathematically Developing Building Facades: An Algorithmic Framework. In *Formal Methods in Architecture*; Eloy, S., Leite Viana, D., Morais, F., Vieira Vaz, J., Eds.; Springer International Publishing: Cham, Switzerland, 2021; pp. 3–17, ISBN 978-3-030-57508-3.
17. Hazbei, M.; Rafati, N.; Kharma, N.; Eicker, U. Optimizing architectural multi-dimensional forms; a hybrid approach integrating approximate evolutionary search, clustering and local optimization. *Energy Build.* **2024**, *318*, 114460. [CrossRef]

18. Ranjazmay Azari, M.; Bemanian, M.; Mahdavinejad, M.; Körner, A.; Knippers, J. Application-based principles of islamic geometric patterns; state-of-the-art, and future trends in computer science/technologies: A review. *Herit. Sci.* **2023**, *11*, 22. [CrossRef]
19. Dastoum, M.; Sanchez Guevara, C.; Arranz, B. Efficient daylighting and thermal performance through tessellation of geometric patterns in building façade: A systematic review. *Energy Sustain. Dev.* **2024**, *83*, 101563. [CrossRef]
20. Emami, N.; Giles, H. Geometric Patterns, Light and Shade: Quantifying Aperture Ratio and Pattern Resolution in the Performance of Shading Screens. *Nexus Netw. J.* **2016**, *18*, 197–222. [CrossRef]
21. Rashwan, A.; El Gizawi, L.; Sheta, S. Evaluation of the effect of integrating building envelopes with parametric patterns on daylighting performance in office spaces in hot-dry climate. *Alex. Eng. J.* **2019**, *58*, 551–557. [CrossRef]
22. Taki, A.; Kumari, H. Examining Mashrabiya's Impact on Energy Efficiency and Cultural Aspects in Saudi Arabia. *Sustainability* **2023**, *15*, 10131. [CrossRef]
23. Bande, L.; Asmelash, Y.; Ahmad, A.; Cyiza, A.; Berengueres, J. Evaluation of an Existing Validated Emirati House versus a New Parametric Design Based on the Local Social Environment through the Application of Advanced Tools. *Buildings* **2023**, *13*, 2627. [CrossRef]
24. Sabry, H.; Sherif, A.; Gadelhak, M.; Aly, M. Balancing the daylighting and energy performance of solar screens in residential desert buildings: Examination of screen axial rotation and opening aspect ratio. *Sol. Energy* **2014**, *103*, 364–377. [CrossRef]
25. Tabadkani, A.; Banihashemi, S.; Hosseini, M.R. Daylighting and visual comfort of oriental sun responsive skins: A parametric analysis. *Build. Simul.* **2018**, *11*, 663–676. [CrossRef]
26. Yi, Y.K. Building facade multi-objective optimization for daylight and aesthetical perception. *Build. Environ.* **2019**, *156*, 178–190. [CrossRef]
27. Lin, C.-H.; Tsay, Y.-S. A metamodel based on intermediary features for daylight performance prediction of façade design. *Build. Environ.* **2021**, *206*, 108371. [CrossRef]
28. Maksoud, A.; Mushtaha, E.; Al-Sadoon, Z.; Sahall, H.; Toutou, A. Design of Islamic Parametric Elevation for Interior, Enclosed Corridors to Optimize Daylighting and Solar Radiation Exposure in a Desert Climate: A Case Study of the University of Sharjah, UAE. *Buildings* **2022**, *12*, 161. [CrossRef]
29. Hosseini, S.M.; Heidari, S. General morphological analysis of Orosi windows and morpho butterfly wing's principles for improving occupant's daylight performance through interactive kinetic façade. *J. Build. Eng.* **2022**, *59*, 105027. [CrossRef]
30. Kızılörenli, E.; Maden, F. Modular responsive facade proposals based on semi-regular and demi-regular tessellation: Daylighting and visual comfort. *Front. Archit. Res.* **2023**, *12*, 601–612. [CrossRef]
31. Kahramanoğlu, B.; Çakıcı Alp, N. Enhancing visual comfort with Miura-ori-based responsive facade model. *J. Build. Eng.* **2023**, *69*, 106241. [CrossRef]
32. Kangazian, A.; Emadian Razavi, S.Z. Multi-criteria evaluation of daylight control systems of office buildings considering daylighting, glare and energy consumption. *Sol. Energy* **2023**, *263*, 111928. [CrossRef]
33. Wen, S.; Hu, X.; Hua, G.; Xue, P.; Lai, D. Comparing the performance of four shading strategies based on a multi-objective genetic algorithm: A case study in a university library. *J. Build. Eng.* **2023**, *63*, 105532. [CrossRef]
34. Dong, Y.; Sun, C.; Han, Y.; Liu, Q. Intelligent optimization: A novel framework to automatize multi-objective optimization of building daylighting and energy performances. *J. Build. Eng.* **2021**, *43*, 102804. [CrossRef]
35. Bianchi, S.; Andriotis, C.; Klein, T.; Overend, M. Multi-criteria design methods in façade engineering: State-of-the-art and future trends. *Build. Environ.* **2024**, *250*, 111184. [CrossRef]
36. Gaber, B.; Zhan, C.; Han, X.; Omar, M.; Li, G. Employing ANN for daylight and energy prediction of hot climate office buildings: A case study of new Cairo, Egypt. *Archit. Eng. Des. Manag.* **2023**, *20*, 1752–1776. [CrossRef]
37. Pinto, M.C.; Crespi, G.; Dell'Anna, F.; Becchio, C. Combining energy dynamic simulation and multi-criteria analysis for supporting investment decisions on smart shading devices in office buildings. *Appl. Energy* **2023**, *332*, 120470. [CrossRef]
38. Almerbati, N.; Ford, P.; Dean, L. Lionel Theodore Dean. In *From Vernacular to Personalised and Sustainable*; Architectural Science Association: Sydney, Australia, 2014.
39. Bagasi, A.A.; Calautit, J.K.; Karban, A.S. Evaluation of the Integration of the Traditional Architectural Element Mashrabiya into the Ventilation Strategy for Buildings in Hot Climates. *Energies* **2021**, *14*, 530. [CrossRef]
40. Lee, J.-Y.; Kim, S.-W.; Jeon, Y.-C. Study of the Control of Geometric Pattern Using Digital Algorithm (with Focus on Analysis and Application of the Islamic Star Pattern). *Adv. Mater. Sci. Eng.* **2015**, *2015*, 950232. [CrossRef]
41. Arrow Metal. Available online: https://www.arrowmetal.com.au/ (accessed on 15 January 2025).
42. McKay, M.D.; Beckman, R.J.; Conover, W.J. A Comparison of Three Methods for Selecting Values of Input Variables in the Analysis of Output from a Computer Code. *Technometrics* **1979**, *21*, 239. [CrossRef]
43. Choi, Y.; Song, D.; Yoon, S.; Koo, J. Comparison of Factorial and Latin Hypercube Sampling Designs for Meta-Models of Building Heating and Cooling Loads. *Energies* **2021**, *14*, 512. [CrossRef]
44. The MathWorks Inc. *MATLAB*, Version R2024b; The MathWorks Inc.: Natick, MA, USA, 2024.

45. Rafati, N.; Hazbei, M.; Eicker, U. Louver configuration comparison in three Canadian cities utilizing NSGA-II. *Build. Environ.* **2023**, *229*, 109939. [CrossRef]
46. Taherdoost, H.; Madanchian, M. Analytic Network Process (ANP) Method: A Comprehensive Review of Applications, Advantages, and Limitations. *J. Data Sci. Intell. Syst.* **2023**, *1*, 12–18. [CrossRef]
47. Magableh, G.; Mistarihi, M. Applications of MCDM approach (ANP-TOPSIS) to evaluate supply chain solutions in the context of COVID-19. *Heliyon* **2022**, *8*, e09062. [CrossRef] [PubMed]
48. *ANSI/ASHRAE Standard 55*; Thermal Environmental Conditions for Human Occupancy. American Society of Heating, Refrigerating and Air-Conditioning Engineers: Peachtree Corners, GA, USA, 2023.
49. Ladybug Tools. Available online: https://www.ladybug.tools/epwmap/ (accessed on 1 October 2024).
50. Li, L.; Qi, Z.; Ma, Q.; Gao, W.; Wei, X. Evolving multi-objective optimization framework for early-stage building design: Improving energy efficiency, daylighting, view quality, and thermal comfort. *Build. Simul.* **2024**, *17*, 2097–2123. [CrossRef]
51. El-Agami, M.; Hanafy, G.; Osman, M. Investigating the Effect of High-Rise Buildings' Mass Geometry on Energy Efficiency within the Climatic Variation of Egypt. *Sustainability* **2021**, *13*, 10529. [CrossRef]
52. Elkhayat, Y.O.; Ibrahim, M.G.; Tokimatsu, K.; Ali, A.A.M. Multi-criteria selection of high-performance glazing systems: A case study of an office building in New Cairo, Egypt. *J. Build. Eng.* **2020**, *32*, 101466. [CrossRef]
53. Kirimtat, A.; Manioğlu, G. A simulation-based performance evaluation of new generation dynamic shading devices with multi-objective optimization. *J. Build. Eng.* **2024**, *90*, 109322. [CrossRef]
54. Lechner, N. *Heating, Cooling, Lighting: Sustainable Design Methods for Architects*, 4th ed.; J. Wiley & Sons: Hoboken, NJ, USA, 2015; ISBN 9781118582428.
55. Choi, J.; Lee, T.; Ahn, E.; Piao, G. Parametric Louver Design System Based On Direct Solar Radiation Control Performance. *J. Asian Archit. Build. Eng.* **2014**, *13*, 57–62. [CrossRef]
56. Toutou, A.; Fikry, M.; Mohamed, W. The parametric based optimization framework daylighting and energy performance in residential buildings in hot arid zone. *Alex. Eng. J.* **2018**, *57*, 3595–3608. [CrossRef]
57. *ASHRAE Standard 90.1-2019*; Energy Standard for Buildings Except Low-Rise Residential Buildings. American Society of Heating, Refrigerating and Air-Conditioning Engineers, Inc: Atlanta, GA, USA, 2019.
58. Nabil, A.; Mardaljevic, J. Useful daylight illuminances: A replacement for daylight factors. *Energy Build.* **2006**, *38*, 905–913. [CrossRef]
59. Wu, C.; Pan, H.; Luo, Z.; Liu, C.; Huang, H. Multi-objective optimization of residential building energy consumption, daylighting, and thermal comfort based on BO-XGBoost-NSGA-II. *Build. Environ.* **2024**, *254*, 111386. [CrossRef]
60. Konis, K.; Gamas, A.; Kensek, K. Passive performance and building form: An optimization framework for early-stage design support. *Sol. Energy* **2016**, *125*, 161–179. [CrossRef]
61. Pilechiha, P.; Mahdavinejad, M.; Pour Rahimian, F.; Carnemolla, P.; Seyedzadeh, S. Multi-objective optimisation framework for designing office windows: Quality of view, daylight and energy efficiency. *Appl. Energy* **2020**, *261*, 114356. [CrossRef]
62. Architectural Energy Corporation. *Daylighting Metric Development Using Daylight Autonomy Calculations in the Sensor Placement Optimization Tool*; CHPS Daylighting Committee, Daylighting Forum: Boulder, CO, USA, 2006.
63. EnergyPlus. Version 9.2. Available online: https://bigladdersoftware.com/epx/docs/9-2/engineering-reference/ (accessed on 1 October 2024).
64. Ayoub, M. A review on machine learning algorithms to predict daylighting inside buildings. *Sol. Energy* **2020**, *202*, 249–275. [CrossRef]
65. Shi, Y. *Cutting-Edge Research Topics on Multiple Criteria Decision Making, Proceedings od the 20th International Conference, MCDM 2009, Chengdu, China, 21–26 June 2009*; Springer: Heidelberg, Germany, 2009; ISBN 978-3-642-02297-5.
66. Omar, M.; Janada, K.; Soltan, H. FAQT: A Precise System for Welding Process Selection. *Int. J. Fuzzy Syst.* **2022**, *24*, 1605–1618. [CrossRef]
67. Li, D.H.; Chau, T.C.; Wan, K.K. A review of the CIE general sky classification approaches. *Renew. Sustain. Energy Rev.* **2014**, *31*, 563–574. [CrossRef]
68. Chen, W.; Li, D.H.; Li, S.; Lou, S. Predicting diffuse solar irradiance on obstructed building façades under irregular skyline patterns for various ISO/CIE standard skies. *J. Build. Eng.* **2021**, *40*, 102370. [CrossRef]
69. Amorim, C.N.D.; Vasquez, N.G.; Matusiak, B.; Kanno, J.; Sokol, N.; Martyniuk-Peczek, J.; Sibilio, S.; Koga, Y.; Ciampi, G.; Waczynska, M. Lighting conditions in home office and occupant's perception: An international study. *Energy Build.* **2022**, *261*, 111957. [CrossRef]
70. Hu, Y.; Luo, M.R.; Yang, Y. A Study on Lighting Uniformity for LED Smart Lighting System. In Proceedings of the 2015 12th China International Forum on Solid State Lighting (SSLCHINA), Shenzhen, China, 2–4 November 2015; pp. 127–130, ISBN 978-1-5090-0175-0.
71. Wienold, J.; Christoffersen, J. Evaluation methods and development of a new glare prediction model for daylight environments with the use of CCD cameras. *Energy Build.* **2006**, *38*, 743–757. [CrossRef]

72. Radiance. Available online: https://www.radiance-online.org/learning/documentation/manual-pages/pdfs/evalglare.pdf/view (accessed on 1 October 2024).
73. Qi, X.; Luo, Z.; Ghahramani, A.; Zhuang, D.; Sun, C. A study of subjective evaluation factors regarding visual effects of daylight in offices using machine learning. *J. Build. Eng.* **2024**, *86*, 108906. [CrossRef]
74. Kumaragurubaran, V.; Inanici, M. Hdrscope: High Dynamic Range Image Processing Toolkit for Lighting Simulations and Analysis. In Proceedings of the BS 2013: 13th Conference of the International Building Performance Simulation Association, Chambery, France, 25–28 August 2013; pp. 3400–3407.